

Article

Evaluation of BRDF Archetypes for Representing Surface Reflectance Anisotropy Using MODIS BRDF Data

Hu Zhang ^{1,2}, Ziti Jiao ^{1,2,*}, Yadong Dong ^{1,2} and Xiaowen Li ^{1,2,†}

¹ State Key Laboratory of Remote Sensing Science, and School of Geography, Beijing Normal University, Beijing 100875, China; E-Mails: askzhanghu@126.com (H.Z.); dyd@mail.bnu.edu.cn (Y.D.); lix@bnu.edu.cn (X.L.)

² Beijing Key Laboratory of Environmental Remote Sensing and Digital City, Beijing Normal University, Beijing 100875, China

† This author has been deceased.

* Author to whom correspondence should be addressed; E-Mail: jiaozt@bnu.edu.cn; Tel.: +86-10-5880-1730; Fax: +86-10-5880-5274.

Academic Editors: Richard Müller and Prasad S. Thenkabail

Received: 12 March 2015 / Accepted: 25 May 2015 / Published: 15 June 2015

Abstract: Bidirectional reflectance distribution function (BRDF) archetypes extracted from the Moderate Resolution Imaging Spectroradiometer (MODIS) BRDF/Albedo product over the global Earth Observing System Land Validation Core Sites can be used to simplify BRDF models. The present study attempts to evaluate the representativeness of BRDF archetypes for surface reflectance anisotropy. Five-year forward-modeled MODIS multi-angular reflectance (MCD-ref) and additional actual MODIS multi-angular observations (MCD-obs) in four growing periods in 2008 over three tiles were taken as validation data. First, BRDF archetypes in the principal plane were qualitatively compared with the time-series MODIS BRDF product of randomly sampled pixels. Secondly, BRDF archetypes were used to fit MCD-ref, and the average root-mean-squared errors (RMSEs) over each tile were examined for these five years. Finally, both BRDF archetypes and the MODIS BRDF were used to fit MCD-obs, and the histograms of the fit-RMSEs were compared. The consistency of the directional reflectance between the BRDF archetypes and MODIS BRDFs in nadir-view, hotspot and entire viewing hemisphere at 30° and 50° solar geometries were also examined. The results confirm that BRDF archetypes are representative of surface reflectance anisotropy for available snow-free MODIS data.

Keywords: bidirectional reflectance distribution function (BRDF); BRDF archetype; albedo; anisotropic flat index; Moderate Resolution Imaging Spectroradiometer (MODIS); prior knowledge; kernel-driven BRDF model

1. Introduction

The Bidirectional Reflectance Distribution Function (BRDF) is defined as the ratio of the reflected radiance in a particular direction to the incident radiation in a particular direction [1]. This ratio varies as a function of sun and sensor geometry and characterizes the surface reflectance anisotropy. The shape and magnitude of BRDF is determined by the structure of the land surface and the optical attributes of the reflecting elements [2,3]. The actual instantaneous BRDF cannot be directly measured but can be estimated by numerical BRDF models and multi-angular measurements with varying sun-view geometries [1,4]. The three parameter semi-empirical RossThick-LiSparse-Reciprocal (RTLSR) BRDF model is one of the most commonly used models for characterizing the anisotropic reflectance of land surfaces [5–7].

Time-series satellite measurements have been used to evaluate and correct the effect of anisotropic reflectance [8,9] and to retrieve surface vegetation structure and other bio-geophysical parameters [5,10]. One of the most important applications of BRDF is the derivation of surface albedos from a limited number of remotely sensed angular samples through the integration of BRDFs over the viewing hemisphere or bi-hemisphere. In recent decades, land surface albedo products that incorporate surface reflectance anisotropy have been derived from satellite sensors at regional and global scales. These products include MODIS [5,6], Multi-angle Imaging Spectro-Radiometer (MISR) [11,12], Polarization and Directionality of the Earth's Reflectances (POLDER) [13,14], Meteosat and Meteosat Second Generation (MSG) [15,16]. With high-quality multi-angular surface reflectance data and the RTLSR BRDF model, MODIS has provided global BRDF/Albedo products at a 500-m spatial resolution since 2000. The high accuracy of the MODIS albedo has been validated with ground-, airborne-, and space-based measurements [17–23]. The MODIS BRDF/Albedo products have been widely utilized by the modeling community [24–26].

Multi-angular observations provided by satellites are restricted by satellite orbits and by the sampling capability of sensors; therefore, these observations usually have limited and relatively fixed samples, and they are insufficient for properly assessing anisotropy patterns at regional and global scales. Many efforts have been undertaken to estimate surface reflectance anisotropies as a priori knowledge *in situ* ations for which sufficient angular observational data are unavailable to characterize the surface anisotropy directly [27–30]. The effects of anisotropic reflectance have been observed for many decades in both field measurements [31–35] and satellite observations [6,14,36]. However, the characteristics of BRDF have not been fully explored and understood. In earlier studies, a series of field measurements of the surface anisotropy [31–35] revealed that BRDFs are associated with different homogeneous land cover types. The earliest version of the MODIS BRDF/Albedo operational backup algorithm (magnitude inversion) [28,37] relied on prescribed BRDF shapes associated with specific land cover types as prior knowledge when insufficient MODIS observations were obtained or

when the internal quality check indicated low confidence in the primary algorithm retrievals. Moreover, other studies have noted that the variability in the BRDF model parameters of several MODIS land cover types was higher within land cover types than between land cover types [38]. Currently, in the Collection V006 MODIS operational BRDF/Albedo algorithm, the BRDF information from the latest full-inversion result at each pixel is used as a priori knowledge in the backup algorithm but remains flagged as low-quality results [20]. Although the operational MODIS processes have the luxury of utilizing historical high quality retrievals as a priori information for a particular pixel, there are situations where more simplified and generalized measures of surface anisotropy are desirable.

Six spectral BRDF archetypes based on the Anisotropic Flat index (AFX) [39] were recently derived from a single year of high-quality MODIS BRDF data over global Earth Observing System Land Validation Core Sites. With an increase in the AFX, the dominant shapes of the BRDF archetypes change from geometric optical scattering to volumetric scattering. Thus, these BRDF archetypes have the potential to classify surface reflectance anisotropy. Furthermore, an algorithm has been developed to use these BRDF archetypes as *a priori* knowledge for improving the surface albedo estimates for crops with small-viewing-angle airborne observations [40].

AFX-based BRDF archetypes offer a new method for capturing the variability in surface reflectance anisotropy. The representativeness of BRDF archetypes for surface reflectance anisotropy requires further assessment by using more sufficient data. The present study supplements the validation using both MCD-ref and MCD-obs prior to further applications of the BRDF archetypes. The similarity between the BRDF archetype and MODIS BRDFs within each BRDF archetype class is measured to assess whether these BRDF archetypes can accurately represent surface reflectance anisotropy.

2. Materials and Methods

Because BRDF archetypes can potentially be used to describe the variability in surface reflectance anisotropy, we further evaluate the representativeness of BRDF archetypes for surface reflectance anisotropy. The flowchart of the evaluation process is shown in Figure 1. MCD-ref and MCD-obs are employed as the validation data in this study. MCD-ref with specific angles is recalculated from MODIS BRDF product, while the MCD-obs is extracted from the MODIS reflectance products (MOD09 and MYD09). Both of these datasets need to be classified into BRDF archetype categories based on their MODIS AFX values. The comparison is conducted as follows: First, the shapes of the BRDF archetypes in the principal plane are qualitatively displayed and compared with the five-year MODIS BRDF product of randomly sampled pixels. Then, the BRDF archetypes are used to fit MCD-ref (Figure 1, module A), and the average root-mean-squared errors (RMSEs) of each tile over five years are also used to assess the similarity between the BRDF archetypes and MODIS BRDFs. Finally, the BRDF archetypes and MODIS BRDF are used to fit MCD-obs (module C), and the histograms of the fit-RMSEs of the BRDF archetypes and MODIS BRDFs in each tile are compared with each other in seven MODIS bands. The forward-modeled directional reflectance at nadir, hotspot and the entire viewing hemisphere over 30° and 50° solar geometries, which are calculated from BRDF archetypes and MODIS BRDF product separately, are also compared.

We must emphasize that the application of these BRDF archetypes in the retrieval of land surface bio-geophysical parameters from limited observational data is an urgent issue. Although the BRDF

archetypes have been successfully used in the albedo retrieval for small-viewing-angle airborne observations [40], for further use of them in improving the accuracy of albedo from insufficient observations in complex inhomogeneous environments still needs more effort. For the further application of these BRDF archetypes, determining whether the BRDF archetypes represent surface reflectance anisotropy is also a key component in the study of surface reflectance anisotropy characteristics. Therefore, in this study, the process of archetype selection simply uses the MODIS AFX to classify MCD-ref and MCD-obs and to select the corresponding BRDF archetype for every pixel (module B).

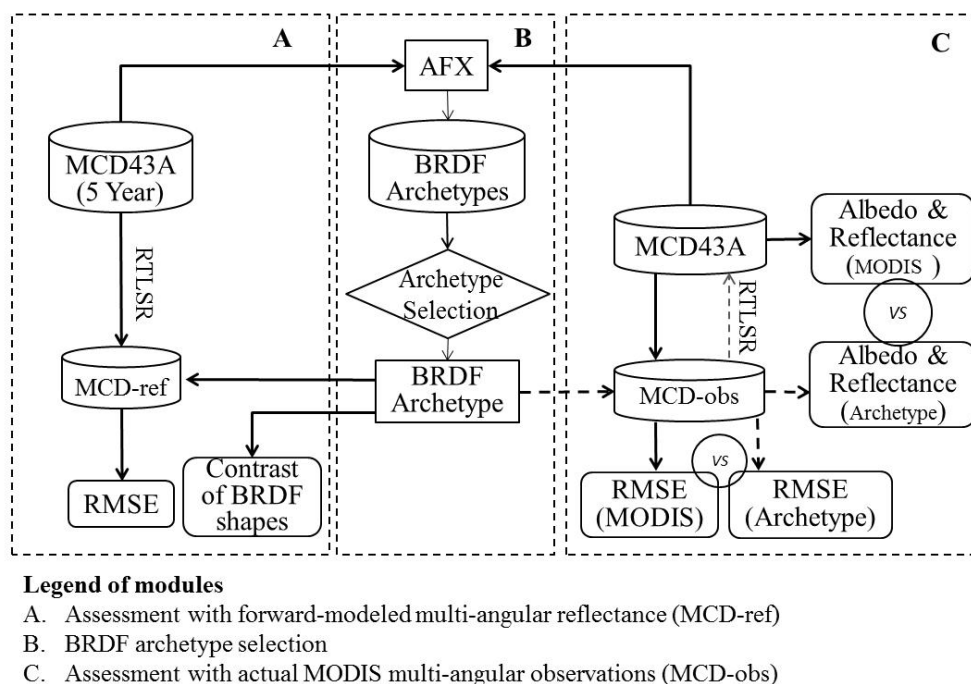


Figure 1. Flowchart for evaluating the representativeness of BRDF archetypes for surface reflectance anisotropy from MODIS data.

2.1. MODIS Data Set

The MODIS surface reflectance products (MOD09GA and MYD09GA) provide an estimate of the narrow-band surface reflectance as it would be measured at the earth's surface without the effect of atmospheric scattering or absorption [41]. Using the RTLSR model and multi-date, clear-sky and atmospherically corrected MODIS surface reflectances over a 16-day period, the BRDF/Albedo product of the global land surface is retrieved at a spatial resolution of 500-m [6]. In this study, a 5-year time series of MODIS BRDF/Albedo products (MCD43A) (2008 to 2012) over tiles H11V03, H08V05 and H20V11 is used to evaluate the representativeness of BRDF archetypes for surface reflectance anisotropy using MODIS BRDF data. In practice, MCD-ref that is recalculated from the RTLSR BRDF model and MODIS BRDF/Albedo product (MCD43A1) is used. In this study, MCD-ref has a 10° interval for the viewing zenith angle and a 15° interval for the viewing azimuth angle in the viewing hemisphere. The specific solar zenith angles (30° and 50°) and the largest viewing zenith angle of 70° are set for MCD-ref.

In addition, MCD-obs over the three tiles in four growing periods (green up, maturity, senescence, and dormancy) in 2008 are also used to assess the representation of BRDF archetypes by MODIS BRDF. MCD-obs are extracted from the MODIS reflectance products (MOD09 and MYD09) over a 16-day period using the operational MODIS BRDF/Albedo algorithm. In order to ensure the high quality of MCD-obs, only the pixels that have high-quality MODIS BRDFs are used in this study. Also note that both MCD-ref and MCD-obs are independent of the data that were used to distill the six spectral BRDF archetypes in the previous study [39].

2.2. Study Area

Five year time series MCD-ref and additional MCD-obs from MODIS tile H11V03, H08V05 and H20V11 are used to evaluate the representativeness of BRDF archetypes for surface reflectance anisotropy. MODIS tile H11V03 is located in northwestern Canada; it contains croplands, evergreen needle forest and mixed forest land. Tile H08V05 is located along the west coast of America with primary land cover types of shrub and grass. This region has a subtropical, hot desert climate, with most precipitation in winter (February is the wettest month of year). Tile H20V11 is located in southern Africa, where the main land cover types are grass, shrubs, and savanna. Although these three tiles cannot capture all characteristics of the surface reflectance anisotropy of the earth's surface, they represent the major forest-shrub-herbaceous land cover types from the Northern Hemisphere to the Southern Hemisphere.

2.3. RTLSR BRDF Model

The semi-empirical RTLSR BRDF model is a linear combination of three basic scattering components: the isotropic scattering fraction, the volumetric scattering fraction and the geometric-optical scattering fraction. The model has the following form [5,42,43]:

$$R(\Omega_i; \Omega_r; \lambda) = f_{iso}(\lambda) + f_{vol}(\lambda)K_{vol}(\Omega_i; \Omega_r) + f_{geo}(\lambda)K_{geo}(\Omega_i; \Omega_r) \quad (1)$$

where the subscripts i and r represent the incident and reflective directions; Ω_i and Ω_r denote the incident and reflective direction vectors; $R(\Omega_i; \Omega_r; \lambda)$ is the bidirectional reflectance distribution function in waveband λ ; $K_{vol}(\Omega_i; \Omega_r)$ and $K_{geo}(\Omega_i; \Omega_r)$ are kernel functions that describe the volumetric and geometric optical scattering; and $f_{iso}(\lambda)$, $f_{vol}(\lambda)$ and $f_{geo}(\lambda)$ are the weights (model parameters) of different types of scattering.

$K_{vol}(\Omega_i; \Omega_r)$ models the reflectance of a theoretical turbid vegetation canopy with high leaf density in the single-scattering approximation [44]. The volumetric kernel is typically bowl shaped with the reflectance increases at large viewing zenith angle in the principal plane. $K_{geo}(\Omega_i; \Omega_r)$ models the reflectance of a flat Lambertian surface covered with randomly distributed spheroids that have the same optical properties as the soil [45]. The geometric optical kernel is typically dome-shaped with the reflectance increases smooth from oblique directions to backscattering in the principal plane. Several studies have shown that the RossThick-LiSparse-Reciprocal kernel combination best fits ground- and satellite- based observations [5,43].

The model parameters that best fit the observations can be obtained through a linear regression analysis in the inversion procedure. Using the model parameters and RTLSR model, we can calculate

the black sky albedo (BSA) and white sky albedo (WSA). Moreover, the directional reflectance under any illumination and viewing geometry can also be reconstructed [6].

2.4. AFX and BRDF Archetype Database

The AFX is defined as the ratio of the WSA to the isotropic parameter f_{iso} as follows [39]:

$$AFX(\lambda) = \frac{WSA}{f_{iso}(\lambda)} = 1 + \frac{f_{vol}(\lambda)}{f_{iso}(\lambda)} \times 0.189184 - \frac{f_{geo}(\lambda)}{f_{iso}(\lambda)} \times 1.377622 \quad (2)$$

where the constants 0.189184 and -1.377622 are the bi-hemispherical integrals of the RossThick kernel and the LiSparse Reciprocal kernel, respectively, and λ represents the band.

The previous study demonstrated that AFX can be used to identify the general characteristics of surface reflectance anisotropy [39]. The BRDF shapes change from dome shaped to bowl shaped in the principal plane with increasing AFX. This characteristic enables the development of a BRDF-based classification scheme for the BRDF typology, and six spectral BRDF archetypes for seven MODIS bands have been derived using the AFX and V005 MODIS BRDF product. Table 1 shows the AFX, BRDF model parameter and normalized BRDF model parameter of the BRDF archetypes in the MODIS red and near-infrared (NIR) bands. Because the spectral reflectance amplitudes of different land surfaces vary, the original MODIS BRDF is normalized by multiplying it by a scale factor of $K = 0.5/f_{iso}$; this process removes the variation and make the BRDFs of different targets comparable. The BRDFs before and after normalization have the same AFX value; therefore, they have the same anisotropic characteristics. Details on establishing BRDF archetypes from available multi-angular observations and BRDF archetypes for seven MODIS bands can be found in [39].

Table 1. AFX and model parameters of six BRDF archetypes in the original (f_{iso} , f_{vol} , f_{geo}) and normalized (F_{iso} , F_{vol} , F_{geo}) forms in the MODIS red and NIR bands.

Band	Archetype Number	AFX Range	AFX	f_{iso}	f_{vol}	f_{geo}	F_{iso}	F_{vol}	F_{geo}
Red	1	[0.382, 0.680]	0.618	0.1424	0.0082	0.0406	0.5	0.0288	0.1426
	2	[0.680, 0.795]	0.736	0.119	0.0305	0.027	0.5	0.1282	0.1134
	3	[0.795, 0.899]	0.843	0.1195	0.0485	0.0202	0.5	0.2029	0.0845
	4	[0.899, 1.026]	0.956	0.1324	0.0816	0.0155	0.5	0.3082	0.0585
	5	[1.026, 1.240]	1.107	0.0893	0.0862	0.0049	0.5	0.4826	0.0274
	6	[1.240, 1.946]	1.386	0.0396	0.086	0.0007	0.5	1.0859	0.0088
NIR	1	[0.541, 0.804]	0.744	0.3148	0.0767	0.069	0.5	0.1218	0.1096
	2	[0.804, 0.896]	0.853	0.2995	0.1424	0.0515	0.5	0.2377	0.086
	3	[0.896, 0.966]	0.931	0.2829	0.1774	0.0384	0.5	0.3135	0.0679
	4	[0.966, 1.042]	1.002	0.2819	0.1985	0.0269	0.5	0.3521	0.0477
	5	[1.042, 1.142]	1.091	0.2763	0.2388	0.0145	0.5	0.4321	0.0262
	6	[1.142, 1.361]	1.203	0.2909	0.3291	0.0023	0.5	0.5657	0.004

2.5. Inversion Method

The method used to adjust the *a priori* BRDF archetype (BRDF') to fit multi-angular observations mainly follows the MODIS magnitude inversion algorithm [28]. For a set of n multi-angular observations (B), the simulated directional reflectance (B') with the same illumination and viewing

geometry as B can be reconstructed using the *a priori* BRDF archetype and the RTLSR model in a forward modeling manner (Equation (1)). A multiplicative factor a that minimizes the difference between B and aB' using the least-mean-squares technique is given as follows:

$$a = \frac{\sum_{k=1}^n B_k B'_k}{\sum_{k=1}^n B'_k B'_k} \quad (3)$$

The BRDF of the surface derived using the corresponding BRDF archetype as *a priori* knowledge can then be determined by

$$\text{BRDF} = a \times \text{BRDF}' \quad (4)$$

The RMSE between BRDF archetypes and the MODIS BRDF is a key indicator in this assessment. The RMSE can be calculated through the use of MCD-ref or MCD-obs (B) and the adjusted reflectance of a BRDF archetype (aB') with the same sun-view geometries as B (Equation (5)). A smaller RMSE indicates greater similarity between the BRDF archetype and the MODIS BRDFs, *i.e.*, more representative BRDF archetypes.

$$\text{RMSE} = \sqrt{\frac{\sum_{k=1}^n (B_k - aB'_k)^2}{n-1}} \quad (5)$$

The BSA (*i.e.*, directional-hemispherical reflectance) and WSA (*i.e.*, bi-hemispherical reflectance) can be calculated as

$$\text{BSA}(\theta, \lambda) = a \times \sum_{k=1}^{k=3} f_k(\lambda) h_k(\theta) \quad (6)$$

$$\text{WSA}(\lambda) = a \times \sum_{k=1}^{k=3} f_k(\lambda) H_k \quad (7)$$

where $h_k(\theta)$ and H_k are the directional-hemispherical and bi-hemispherical integrals, respectively, of the BRDF model kernels.

3. Result

3.1. Assessment with Time-Series MODIS BRDF Shapes

According to the MODIS AFX typology, we assume that all BRDF shapes belong to one of the six BRDF archetype classes. The high-quality MODIS BRDFs from the five-year time-series data of 1000 randomly sampled pixels in each tile are classified in terms of their MODIS AFX values. BRDF archetypes in the principal plane are qualitatively compared with the corresponding MODIS BRDFs. The normalized BRDF shapes of both BRDF archetypes and the corresponding MODIS BRDFs at a solar zenith angle of 30° in the principal plane in the red and NIR bands from tile H20V11 are shown in Figures 2 and 3. The results of the remaining tiles and bands are similar. Under this illumination geometry, the scattering pattern of both the BRDF archetype and the MODIS BRDFs change slightly from dome shaped (geometric-optical scattering dominated) to bowl shaped (volumetric scattering dominated) with an increasing AFX. The discreteness of the MODIS BRDF shapes within individual

BRDF archetypal classes is most likely caused by the non-orthogonality of the kernel functions in the RTLSR BRDF model [5,39]. Because the variation of volumetric parameters is more remarkable in comparison with geometric parameters, the normalized BRDFs have a much larger fluctuation in the forward scattering direction than the backward. The corresponding BRDF archetype is used to fit MCD-ref that are reconstructed from the original MODIS BRDF product using the method described above. The fit-RMSEs (Equation (5)) between MCD-ref and the reflectances of the adjusted BRDF archetypes with the same illumination and viewing geometries are used to evaluate the fitting ability and representativeness of the BRDF archetypes. Although Figures 2 and 3 show that the normalized MODIS BRDFs are not identical to the normalized BRDF archetypes and that there are no clearly boundaries between the BRDF archetype classes, the average fit-RMSEs of each BRDF archetype class are less than 0.007 and 0.015 in the red and NIR bands, respectively. Therefore, the six spectral BRDF archetypes can capture the major variabilities in the surface reflectance anisotropy of available MODIS BRDF data.

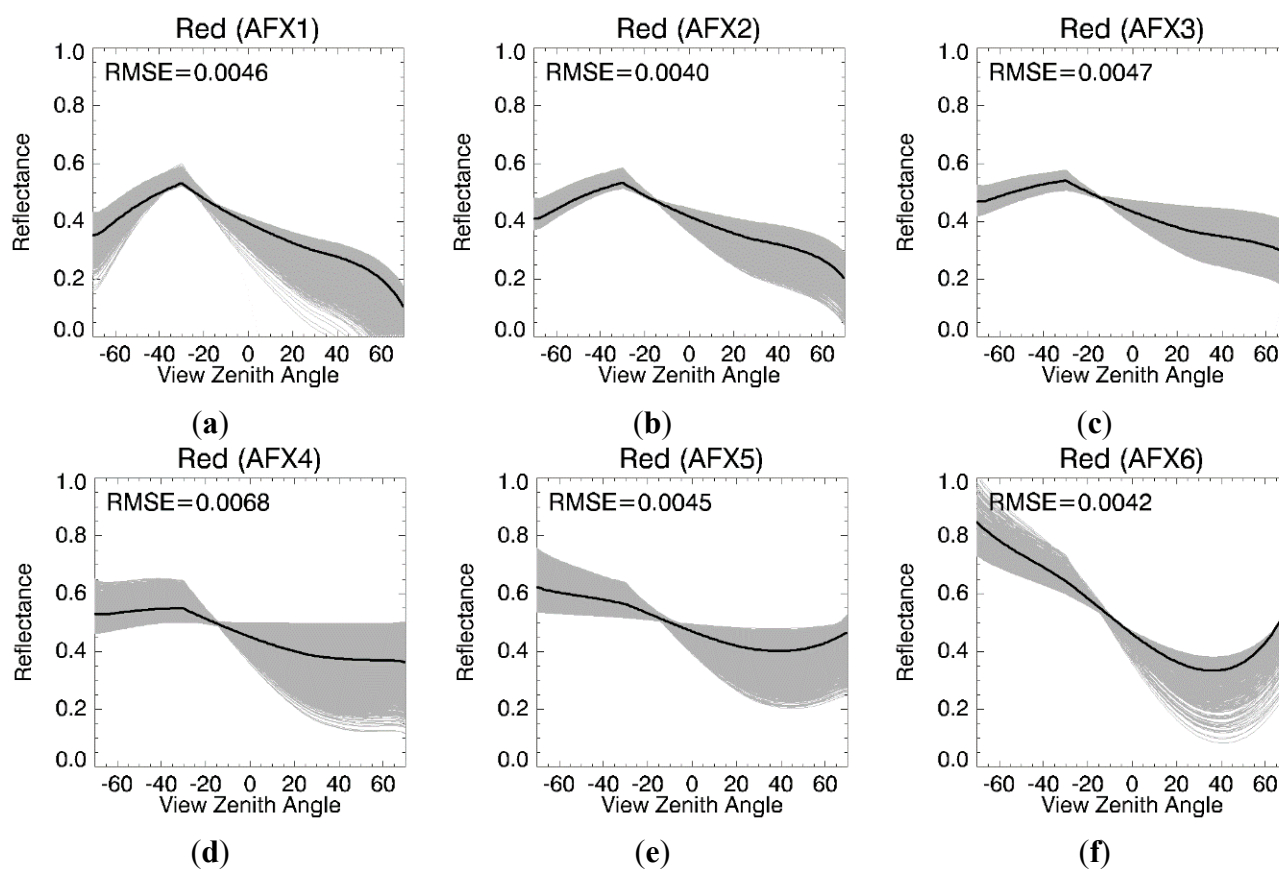


Figure 2. BRDF shapes of the normalized MODIS BRDFs of five-year time-series data of 1000 randomly sampled pixels (grey lines) for tile H20V11 and the corresponding BRDF archetype (black lines) in the principal plane at a solar zenith angle of 30° for the MODIS red band. (a–f) refer to the first–sixth BRDF archetypes. Positive and negative view zenith angles stand for forward and backward scattering direction respectively.

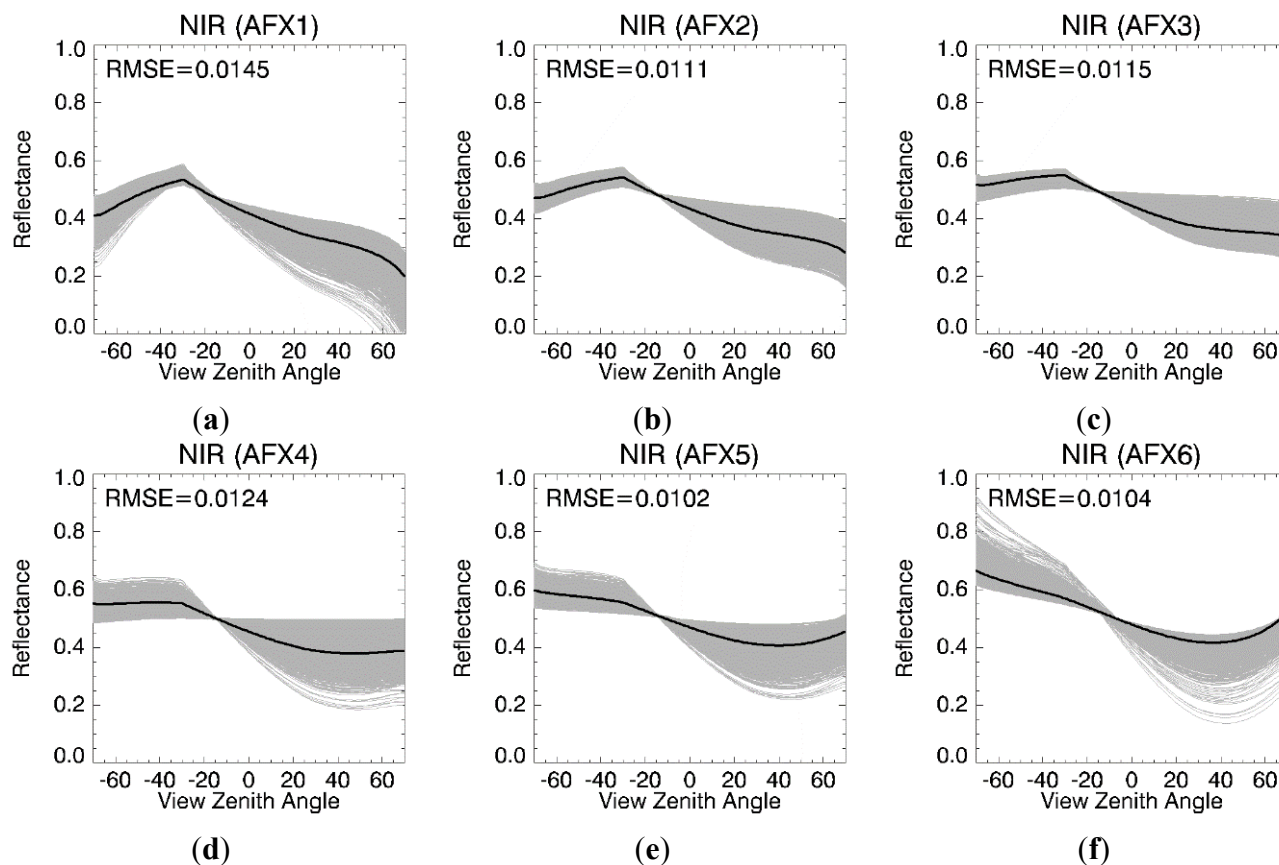


Figure 3. BRDF shapes of the normalized MODIS BRDFs of five-year time-series data of 1000 randomly sampled pixels for tile H20v11 and the corresponding BRDF archetype in the principal plane at a solar zenith angle of 30° for the MODIS NIR band. (a–f) refer to the first–sixth BRDF archetypes.

3.2. Assessment with Time Series MODIS Simulated Reflectance (MCD-ref)

To fully and comprehensively evaluate the representativeness of the six spectral BRDF archetypes for surface reflectance anisotropy, the corresponding BRDF archetype is used to fit MCD-ref of each pixel from three tiles for five years. To eliminate the effect of varying solar zenith angles, a fixed solar zenith angle of 50° is used for the simulated multi-angular reflectance. The average fit-RMSEs of each tile from 2008 to 2012 in the red and NIR bands are shown in Figure 4. Because the reflectance anisotropy characteristics of snow-covered surfaces are not considered in the present BRDF archetypes [39], the fit-RMSEs of snow-covered surfaces are relatively large (solid lines) for tile H11V03. Every February, when the land surface is completely covered with snow and small variations occur during the observation period, the fit-RMSEs are highest (~ 0.1). For these snow-covered surfaces, the fit-RMSEs are subject to the same conditions in the red and near-infrared bands because they have the same magnitude of reflectance. When only the snow-free surface is considered, the fit-RMSEs (dashed lines) decrease (certain days do not have results due to the limited number of snow-free pixels). Tiles H08V05 and H20V11 rarely include snow-covered surfaces during winter, and the average fit-RMSEs of the snow-free surface is maintained at a reasonably low and stable level (< 0.02) for the five years, while the fit-RMSE threshold of 0–0.1 implies a high-quality result in the MODIS operational algorithm [37].

The average fit-RMSE of each tile varies by tiles, bands and growing period. Figure 4b demonstrates differences of up to a factor of 2 for the two tiles in both bands. Notably, the magnitude of the fit-RMSE and the reflectance is positively correlated. The reflectivity of bare soil and sparse vegetation surfaces is higher than that of vegetated surfaces, and vegetated surfaces usually have a high reflectivity in the near-infrared band and a low reflectivity in the red band. Therefore, the fit-RMSE of the near-infrared band is larger than that of the red band, and the fit-RMSEs of tile H08V05 are larger than those of tile H20V11 because tile H08V05 has less vegetation. Moreover, Figures 2 and 3 also show that the fitting abilities of each BRDF archetype are unequal because the fit-RMSEs of each BRDF archetype are not equal. The scattering characteristics of the underlying surface vary with the structure of ground vegetation; therefore, the proportions of each BRDF archetype in the two tiles vary by season. This result also affects the value of the fit-RMSE.

In addition to these results, the albedos retrieved from BRDF archetypes and MCD-ref are highly consistent with the MODIS albedo product, with a determination coefficient near 1, although we do not elaborate upon these results here. These small and stable RMSEs and similar albedos indicate that the six spectral BRDF archetypes can describe various MODIS BRDF shapes of snow-free surfaces from the three tiles in the five-year period.

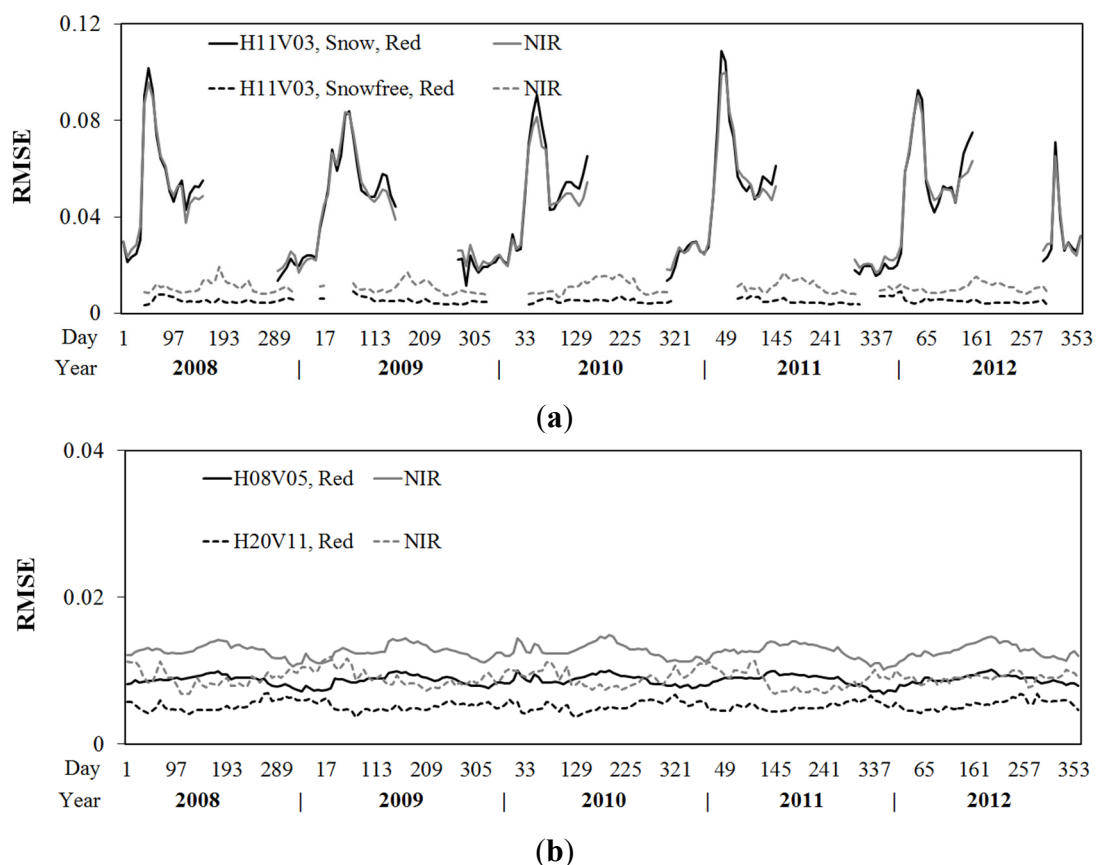


Figure 4. The average fit-RMSEs of (a) tile H11V03 and (b) tile H08V05, H20V11 calculated from BRDF archetypes from 2008 to 2012 in the red (black lines) and NIR (grey lines) bands. The solid lines in (a) refer to the results of the snow-covered surface from tile H11V03.

3.3. Assessment with Actual MODIS Multi-Angular Observations (MCD-obs)

To evaluate the representativeness of BRDF archetypes for surface reflectance anisotropy, the corresponding BRDF archetype is adjusted to fit MCD-obs for three tiles in four growing periods. The fit-RMSE, albedo and specific directional reflectance can be obtained using the above-mentioned method. The fit-RMSE is one of the quality control flags in the MODIS operational BRDF/Albedo algorithm [37] but is not present in routine MODIS BRDF products. To compare the consistency of BRDF archetypes and MODIS BRDFs, the forward-modeled multi-angular reflectance with the same sun-view geometries as the MODIS observations is recalculated from the MODIS BRDF product and RTLSR BRDF model (Equation (1)). The RMSEs between the two reflectances are compared with the RMSEs of the BRDF archetypes. In addition, the albedos and specific directional reflectances that are calculated from the adjusted BRDF archetypes are also compared with the MODIS BRDF/Albedo product or their inversions.

The histograms of the RMSEs for tile H20V11 in seven MODIS bands at four growth stages are shown in Figure 5. Although the fit-RMSEs of BRDF archetypes are slightly larger than the fit-RMSEs of the MODIS BRDF product, the two histograms of the RMSEs in the seven bands are similar. The results for tiles H11V03 and H08V05 are similar to the result for tile H20V11. These results also indicate that MCD-obs with potential noise are not significantly different from the routine MODIS BRDF product in this evaluation. Notably, various high RMSEs (>0.05) are mainly attributed to the observation noise caused by aerosol and sub-pixel cloud contamination during the observation period. The distribution of the RMSE confirms that the BRDF archetypes are close to the corresponding MODIS BRDFs.

The albedos (BSA and WSA) retrieved from the available multi-angular observations and BRDF archetypes are very similar to those of the MODIS albedo product. The determination coefficient is greater than 0.98, and the bias is approximately 0; we do not elaborate upon the albedos here. The albedo is an integration of the BRDF over the viewing hemisphere or bi-hemisphere [5,6]. This process may remove the effect of surface reflectance anisotropy on the albedo and make the two albedos highly consistent. In addition, the fit-RMSE of the BRDF archetype is an overall indicator of the assessment. To obtain additional details on the fitting situation, the reflectance calculated from the adjusted BRDF archetype and MODIS BRDF at nadir (the observation angle is zero) and the hotspot (the scattering angle is zero where the illumination and observation angles coincide) are compared. Figure 6 presents the comparison using the MCD-obs for tiles H11V03 (year 2008, day 137), H08V05 (day 49) and H20V11 (day 249). A solar zenith angle of 30° is used for the forward-modeled reflectance. Similar to the albedo, the nadir reflectances of the adjusted BRDF archetypes under this geometry are similar to the MODIS BRDF inversion with a determination coefficient greater than 0.98. The BRDF archetype inversions include various outliers, which most likely result from noise in the observation caused by the sub-pixel cloud and residual aerosols contamination. These outliers can be effectively removed or assigned a lower weight by the quality assurance technique in the operational MODIS BRDF/albedo algorithm [6,37]. In the hotspot direction, the reflectance of the adjusted BRDF archetypes tends to show slight discreteness with the MODIS inversion, which indicates a weak fitting situation of the BRDF archetypes around this area; however, the difference is not very significant, with a determination coefficient greater than 0.94. The fact that the RTLSR BRDF model and BRDF archetypes consistently underestimate the hotspot observations may contribute to the discreteness [5,43].

Figure 6 shows that the RMSEs between the directional reflectance of the MODIS BRDF inversion and the BRDF archetype inversion can indicate how well the BRDF archetype matches the MODIS BRDF in a particular direction. A larger RMSE corresponds to a poorer consistency. Figure 7 shows the distribution of the RMSE between these two forward-modeled reflectances from the MODIS BRDF and BRDF archetypes at solar zenith angle of 30° and 50° for the entire viewing hemisphere. These RMSEs are also calculated from the multi-angular observations in the three tiles used in Figure 6. The RMSEs are usually relatively large around the hotspot and at large viewing-zenith-angle areas close to the principal plane; moreover the RMSE increase with the increasing solar zenith angle. Around the cross principal plane, the RMSEs are always small. The limited fitting capacity of the RTLSR model around the hotspot area [5,43] and the larger viewing zenith angle [28] partly explains this performance. Tile H08V05 has a greater RMSE than the other two tiles in both bands, which coincides with Figures 4 and 6. The differences mainly originate from the different surface conditions and discrepant proportion of each BRDF archetype over the study area. These results indicate that, except for the hotspot and large viewing-zenith-angle areas, the BRDF archetype can match the BRDF archetype quite well, particularly when the solar zenith angle is small and near the cross principal plane area.

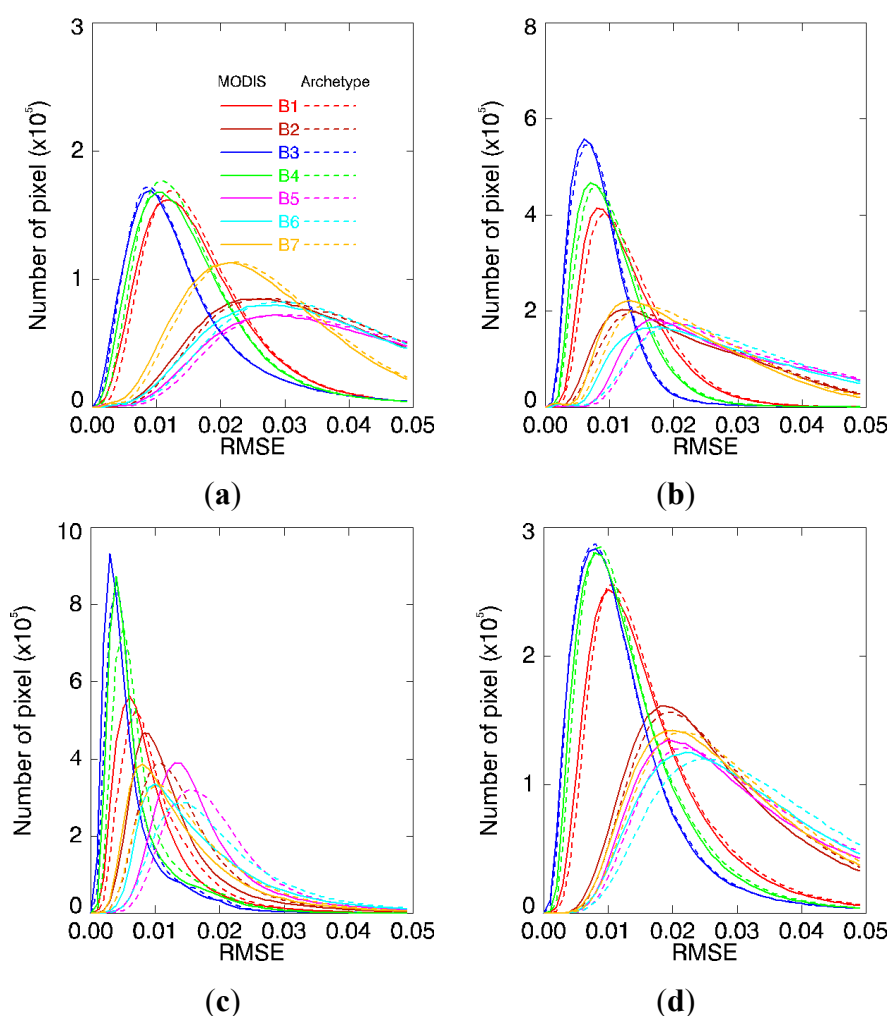


Figure 5. Histograms of RMSEs of the MODIS BRDF product (solid lines) and BRDF archetypes (dashed line) in seven MODIS bands (B1-B7) for 2008, (a) day 65; (b) day 129; (c) day 249; and (d) day 329 for tile H20V11.

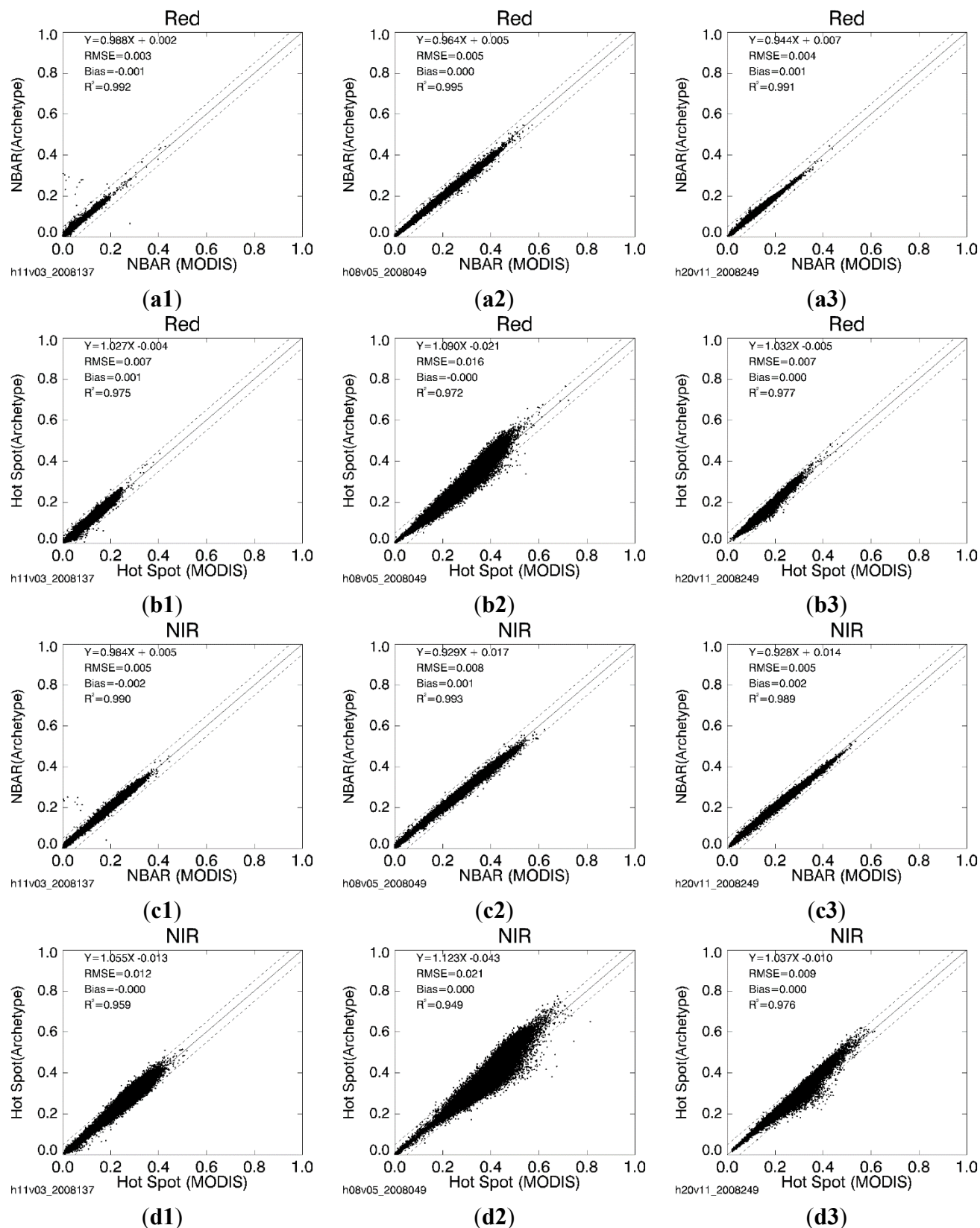


Figure 6. Comparisons of directional reflectance in the (a,b) red and (c,d) NIR bands in the (a, c) nadir-view and (b, d) hotspot directions. Reflectances are retrieved from the adjusted BRDF archetypes (y-axis) and MODIS BRDFs (x-axis) for tiles H11V03 (1st column, year 2008, day 137), H08V05 (2nd column, day 49) and H20V11 (3rd column, day 249).

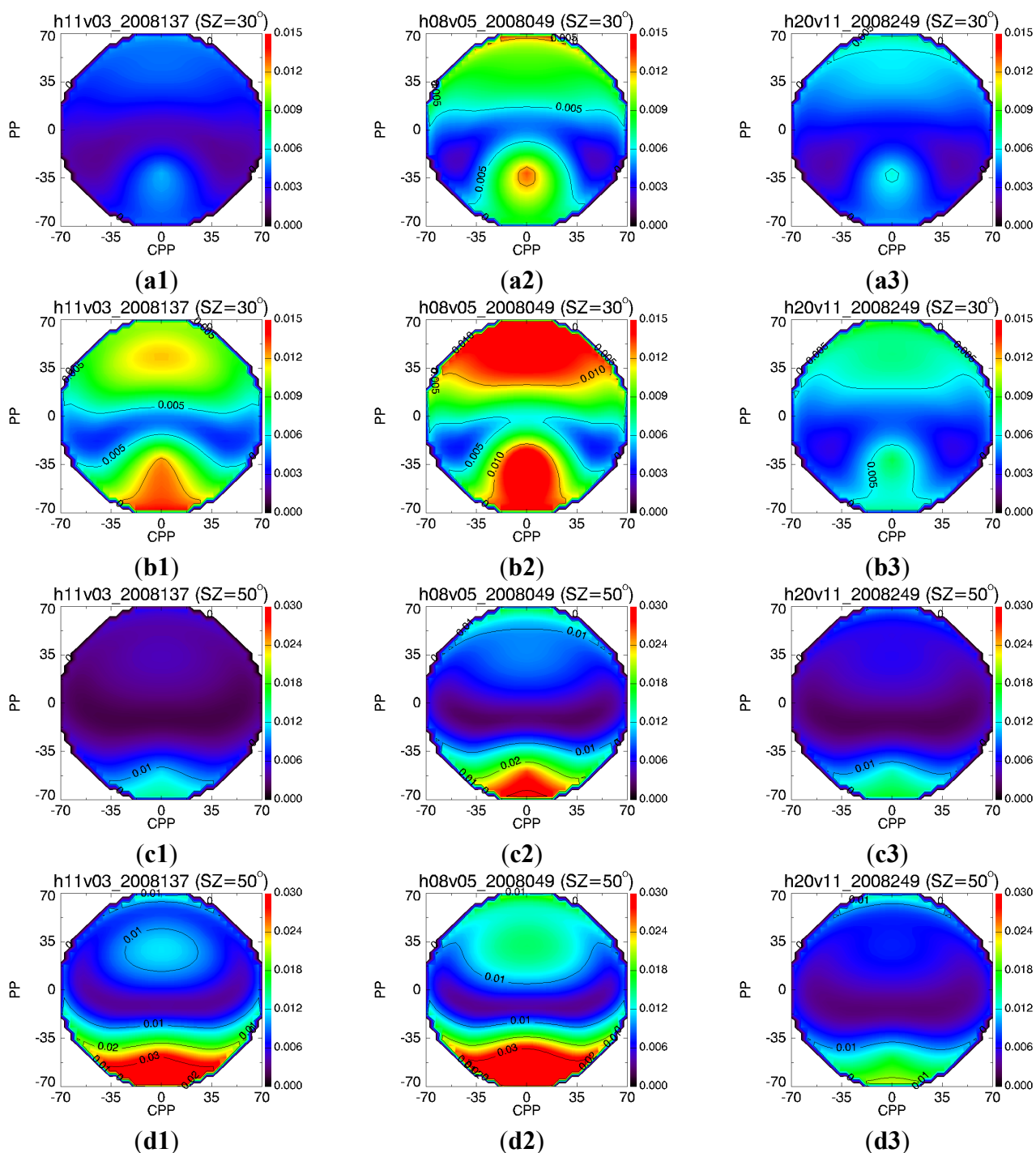


Figure 7. The distribution of RMSEs between the directional reflectance of the MODIS BRDF and the BRDF archetype inversion for the entire viewing hemisphere using MODIS multi-angular observations of tiles H11V03 (1st column, year 2008, day 137), H08V05 (2nd column, day 49) and H20V11 (3rd column, day 249). The solar zenith angles are (a, b) 30° and (c, d) 50° for the (a, c) red and (b, d) NIR bands. The zero zenith angle is in the centre, the radius represents the zenith angle, and the polar angle represents the azimuth angle. The contours and colors represent the values of the RMSE.

4. Discussion

Six spectral BRDF archetypes are extracted from a single year of the MODIS BRDF/Albedo product over the global Earth Observing System Land Validation Core Sites. The BRDF archetypes may simplify the BRDF models and improve the understanding of complex surface reflectance anisotropy. A practical application of these BRDF archetypes has been performed for improving surface albedo retrievals from small-viewing-angle airborne observations [40]. The present study focuses on comprehensively evaluating the ability of several spectral BRDF archetypes to represent surface reflectance anisotropy in a complex environment. In this study, a five-year MODIS BRDF/Albedo product and additional MCD-obs from three tiles are used. The former product is retrieved from high-quality multi-angular observations from Terra and Aqua and has been thoroughly validated [17–23]; the latter is extracted using the operational MODIS BRDF/Albedo code to consider potential noises. The three MODIS tiles used in this study represent major forest-shrub-herbaceous land cover types from the Northern Hemisphere to the Southern Hemisphere and contain the major surface land cover types of the earth's surface. These MCD-ref and MCD-obs within each BRDF archetypal class are used to evaluate the representativeness of corresponding BRDF archetypes.

The representativeness of these BRDF archetypes for surface reflectance anisotropy is first assessed with the 5-year MODIS BRDF/Albedo products. The small bias of the RMSEs between the BRDF archetypes and the MODIS BRDFs indicates that these spectral BRDF archetypes can capture the major variabilities in surface reflectance anisotropy using available MODIS BRDFs. The comparison also shows that the MODIS BRDFs have a reasonable deviation within the BRDF archetype categories. This behavior is most likely a result of the non-orthogonality of the kernel functions in the RTLSR BRDF model [5,39]. The small average RMSEs over each tile between MCD-ref and the corresponding adjusted BRDF archetype for five years over snow-free surfaces also demonstrates that the six BRDF archetypes are representative of surface reflectance anisotropy using the available MODIS data. The relatively large RMSE over snow-covered surfaces indicates that the BRDF archetypes poorly represent the anisotropic characteristics of snow-covered surfaces. Therefore, the current BRDF archetypes require further development to include snow surfaces.

To consider the potential random noise, the representation of these BRDF archetypes is also assessed with MCD-obs in four growing periods in 2008. Such an analysis has not been performed for all time-series data in this study due to processing difficulties in extracting MODIS multi-angular observations. The fit-RMSE histograms of the BRDF archetypes and the MODIS BRDFs are similar. The BSA and WSA retrieved from the BRDF archetypes are highly consistent with the MODIS BRDF/Albedo product. These results indicate that MCD-obs with potential noise are not significantly different than the routine MODIS BRDF product in this evaluation. The forward-modeled reflectance in the nadir direction from the MODIS BRDF and the BRDF archetype are highly consistent with each other. Thus, the BRDF archetype well fits the MODIS BRDF around the nadir area under this specific illumination geometry and may benefit studies of BRDF correction using multi-angular observations. However, these two forward-modeled reflectances in the hotspot direction show some discrete reflectances. Both the RTLSR BRDF model and the BRDF archetypes consistently underestimate the hotspot observations [5,43], and the relatively weak fitting ability of the RTLSR model at large viewing zenith angles [5] may contribute to the discrete reflectance and large RMSE around the

hotspot and large viewing-zenith-angle area. The small RMSEs between the two forward-modeled reflectances over the entire hemisphere under two illumination geometries show that the BRDF archetype matches the MODIS BRDF in the red and NIR bands quite well, particularly when the solar zenith angle is small and near the cross principal plane area.

BRDF archetypes offer a feasible method for categorizing surface reflectance anisotropy, which is, in return, associated with many land surface bio-geophysical parameters [39]. Although, current efforts demonstrate that these BRDF archetypes can capture the major variability in surface reflectance anisotropy from MODIS, additional validations may still be needed using other satellite data, particularly from different sensors with varying spatial resolutions. Recently, two additional methods [46,47] have been developed to address the disaggregation of the MODIS BRDF for retrieving Landsat albedos. We recognize that further examining the BRDF shapes in relation to land cover and NDVI deserves attention in the near future. This study also indicates that further efforts to extract snow-surface BRDF archetypes are also necessary.

5. Conclusions

In this study, we evaluated the representativeness of several BRDF archetypes for surface reflectance anisotropy from MODIS through the use of a five-year MCD-ref retrieved from the MODIS BRDF/Albedo product and additional MCD-obs extracted using operational MODIS BRDF/Albedo codes. The shapes of the BRDF archetype can capture the primary characteristics of the MODIS BRDF, with RMSEs of less than 0.007 and 0.015 in the red and NIR bands, respectively, for each BRDF archetype category. For the snow-free land cover types explored in this study, the average fit-RMSEs are relatively stable during 2008–2012 and are generally less than 0.015 in the red and NIR bands using MCD-ref over tile. However, particular fit-RMSEs are up to 0.05 in seven MODIS bands using MCD-obs, most likely due to random noise in the observations. For snow surfaces, the average fit-RMSEs can be as large as 0.1, indicating a need for further extracting BRDF archetypes from snow surfaces in the near future. The RMSE histograms between the MODIS BRDF and BRDF archetype do not present significant differences. This indicates that it is enough to use the MODIS BRDF product alone and thus may be unnecessary to extract more realistic MODIS multi-angular observations in evaluating these BRDF archetypes. A further examination indicates that intrinsic albedos and nadir reflectances derived from BRDF archetypes are highly consistent with MODIS BRDF/Albedo products ($R^2 > 0.98$), while the reflectances in the hotspot direction and large view zenith angle ($>70^\circ$) present somewhat large variances. This study concludes that these BRDF archetypes can capture the major variability in reflectance anisotropy for MODIS snow-free land cover explored here.

Acknowledgments

This work was supported by the National Basic Research Program (973 Program, 2013CB733400), the NSFC (41171261) and the National High-tech Research and Development Program (863 Program, 2012AA12A304). The authors wish to thank the MODIS team for providing BRDF/Albedo products that are available online.

Author Contributions

Ziti Jiao and Xiaowen Li conceived and designed the research and performed the analyses. Hu Zhang analyzed the data and wrote the original manuscript. Ziti Jiao and Yadong Dong reviewed and edited the manuscript. All authors read and approved the manuscript.

Conflicts of Interest

The authors declare no conflict of interest.

References

1. Nicodemus, F.E.; Richmond, J.C.; Hsia, J.J.; Ginsberg, I.W.; Limperis, T. *Geometrical Considerations and Nomenclature for Reflectance*; National Bureau of Standards, US Department of Commerce: Washington, DC, USA, 1977.
2. Chen, J.M.; Li, X.; Nilson, T.; Strahler, A. Recent advances in geometrical optical modelling and its applications. *Remote Sens. Rev.* **2000**, *18*, 227–262.
3. Strahler, A.H. Vegetation canopy reflectance modeling—Recent developments and remote sensing perspectives. *Remote Sens. Rev.* **1997**, *15*, 179–194.
4. Schaepman-Strub, G.; Schaepman, M.E.; Painter, T.H.; Dangel, S.; Martonchik, J.V. Reflectance quantities in optical remote sensing—Definitions and case studies. *Remote Sens. Environ.* **2006**, *103*, 27–42.
5. Lucht, W.; Schaaf, C.B.; Strahler, A.H. An algorithm for the retrieval of albedo from space using semiempirical BRDF models. *IEEE Trans. Geosci. Remote Sens.* **2000**, *38*, 977–998.
6. Schaaf, C.B.; Gao, F.; Strahler, A.H.; Lucht, W.; Li, X.; Tsang, T.; Strugnell, N.C.; Zhang, X.; Jin, Y.; Muller, J.-P.; *et al.* First operational BRDF, albedo nadir reflectance products from MODIS. *Remote Sens. Environ.* **2002**, *83*, 135–148.
7. Wanner, W.; Strahler, A.H.; Hu, B.; Lewis, P.; Muller, J.P.; Li, X.; Schaaf, C.L.B.; Barnsley, M.J. Global retrieval of bidirectional reflectance and albedo over land from EOS MODIS and MISR data: Theory and algorithm. *J. Geophys. Res.* **1997**, *102*, 17143–17161.
8. Leroy, M.; Hautecoeur, O. Anisotropy-corrected vegetation indexes derived from POLDER/ADEOS. *IEEE Trans. Geosci. Remote Sens.* **1999**, *37*, 1698–1708.
9. Shepherd, J.D.; Dymond, J.R. BRDF correction of vegetation in AVHRR imagery. *Remote Sens. Environ.* **2000**, *74*, 397–408.
10. Roujean, J.-L.; Tanré, D.; Bréon, F.-M.; Deuzé, J.-L. Retrieval of land surface parameters from airborne POLDER bidirectional reflectance distribution function during HAPEX-Sahel. *J. Geophys. Res.* **1997**, *102*, 11201–11218.
11. Martonchik, J.V.; Diner, D.J.; Kahn, R.A.; Ackerman, T.P.; Verstraete, M.E.; Pinty, B.; Gordon, H.R. Techniques for the retrieval of aerosol properties over land and ocean using multiangle imaging. *IEEE Trans. Geosci. Remote Sens.* **1998**, *36*, 1212–1227.
12. Martonchik, J.V.; Diner, D.J.; Pinty, B.; Verstraete, M.M.; Myneni, R.B.; Knyazikhin, Y.; Gordon, H.R. Determination of land and ocean reflective, radiative, and biophysical properties using multiangle imaging. *IEEE Trans. Geosci. Remote Sens.* **1998**, *36*, 1266–1281.

13. Hautecœur, O.; Leroy, M.M. Surface bidirectional reflectance distribution function observed at global scale by POLDER/ADEOS. *Geophys. Res. Lett.* **1998**, *25*, 4197–4200.
14. Leroy, M.; Deuze, J.L.; Breon, F.M.; Hautecœur, O.; Herman, M.; Buriez, J.C.; Tanre, D.; Bouffies, S.; Chazette, P.; Roujean, J.L. Retrieval of atmospheric properties and surface bidirectional reflectances over land from POLDER/ADEOS. *J. Geophys. Res. Atmos.* **1997**, *102*, 17023–17037.
15. Pinty, B.; Roveda, F.; Verstraete, M.M.; Gobron, N.; Govaerts, Y.; Martonchik, J.V.; Diner, D.J.; Kahn, R.A. Surface albedo retrieval from meteosat—1. Theory. *J. Geophys. Res.: Atmos.* **2000**, *105*, 18099–18112.
16. Pinty, B.; Roveda, F.; Verstraete, M.M.; Gobron, N.; Govaerts, Y.; Martonchik, J.V.; Diner, D.J.; Kahn, R.A. Surface albedo retrieval from meteosat—2. Applications. *J. Geophys. Res.: Atmos.* **2000**, *105*, 18113–18134.
17. Liang, S.; Fang, H.; Chen, M.; Shuey, C.J.; Walthall, C.; Daughtry, C.; Morisette, J.; Schaaf, C.; Strahler, A. Validating MODIS land surface reflectance and albedo products: Methods and preliminary results. *Remote Sens. Environ.* **2002**, *83*, 149–162.
18. Salomon, J.G.; Schaaf, C.B.; Strahler, A.H.; Gao, F.; Jin, Y.F. Validation of the MODIS bidirectional reflectance distribution function and albedo retrievals using combined observations from the aqua and terra platforms. *IEEE Trans. Geosci. Remote Sens.* **2006**, *44*, 1555–1565.
19. Liu, J.; Schaaf, C.; Strahler, A.; Jiao, Z.; Shuai, Y.; Zhang, Q.; Roman, M.; Augustine, J.A.; Dutton, E.G. Validation of moderate resolution imaging spectroradiometer (MODIS) albedo retrieval algorithm: Dependence of albedo on solar zenith angle. *J. Geophys. Res.* **2009**, *114*, doi:10.1029/2008JD009969.
20. Wang, Z.; Schaaf, C.B.; Chopping, M.J.; Strahler, A.H.; Wang, J.; Román, M.O.; Rocha, A.V.; Woodcock, C.E.; Shuai, Y. Evaluation of moderate-resolution imaging spectroradiometer (MODIS) snow albedo product (MCD43A) over tundra. *Remote Sens. Environ.* **2012**, *117*, 264–280.
21. Wang, Z.; Schaaf, C.B.; Strahler, A.H.; Chopping, M.J.; Román, M.O.; Shuai, Y.; Woodcock, C.E.; Hollinger, D.Y.; Fitzjarrald, D.R. Evaluation of MODIS albedo product (MCD43A) over grassland, agriculture and forest surface types during dormant and snow-covered periods. *Remote Sens. Environ.* **2014**, *140*, 60–77.
22. Roman, M.O.; Gatebe, C.K.; Yanmin, S.; Zhuosen, W.; Feng, G.; Masek, J.G.; Tao, H.; Shunlin, L.; Schaaf, C.B. Use of *in situ* and airborne multiangle data to assess MODIS- and Landsat-based estimates of directional reflectance and albedo. *IEEE Trans. Geosci. Remote Sens.* **2013**, *51*, 1393–1404.
23. Roman, M.O.; Schaaf, C.B.; Woodcock, C.E.; Strahler, A.H.; Yang, X.; Braswell, R.H.; Curtis, P.S.; Davis, K.J.; Dragoni, D.; Goulden, M.L.; *et al.* The MODIS (collection v005) BRDF/albedo product: Assessment of spatial representativeness over forested landscapes. *Remote Sens. Environ.* **2009**, *113*, 2476–2498.
24. Oleson, K.W.; Bonan, G.B.; Schaaf, C.; Gao, F.; Jin, Y.; Strahler, A. Assessment of global climate model land surface albedo using MODIS data. *Geophys. Res. Lett.* **2003**, *30*, 1443.
25. Tian, Y.; Dickinson, R.E.; Zhou, L.; Myneni, R.B.; Friedl, M.; Schaaf, C.B.; Carroll, M.; Gao, F. Land boundary conditions from MODIS data and consequences for the albedo of a climate model. *Geophys. Res. Lett.* **2004**, *31*, L05504.

26. Myhre, G.; Kvalevåg, M.M.; Schaaf, C.B. Radiative forcing due to anthropogenic vegetation change based on MODIS surface albedo data. *Geophys. Res. Lett.* **2005**, *32*, L21410.
27. Li, X.; Gao, F.; Wang, J.; Strahler, A. A priori knowledge accumulation and its application to linear BRDF model inversion. *J. Geophys. Res.* **2001**, *106*, 11925–11935.
28. Strugnell, N.C.; Lucht, W. An algorithm to infer continental-scale albedo from AVHRR data, land cover class, and field observations of typical BRDFs. *J. Clim.* **2001**, *14*, 1360–1376.
29. Cui, Y.; Mitomi, Y.; Takamura, T. An empirical anisotropy correction model for estimating land surface albedo for radiation budget studies. *Remote Sens. Environ.* **2009**, *113*, 24–39.
30. Jin, Y.; Gao, F.; Schaaf, C.B.; Li, X.; Strahler, A.H.; Bruegge, C.J.; Martonchik, J.V. Improving MODIS surface BRDF/albedo retrieval with MISR multiangle observations. *IEEE Trans. Geosci. Remote Sens.* **2002**, *40*, 1593–1604.
31. Deering, D.W.; Eck, T.F.; Grier, T. Shinnery oak bidirectional reflectance properties and canopy model inversion. *IEEE Trans. Geosci. Remote Sens.* **1992**, *30*, 339–348.
32. Deering, D.W.; Middleton, E.M.; Eck, T.F. Reflectance anisotropy for a spruce-hemlock forest canopy. *Remote Sens. Environ.* **1994**, *47*, 242–260.
33. Deering, D.W.; Middleton, E.M.; Irons, J.R.; Blad, B.L.; Waltershea, E.A.; Hays, C.J.; Walthall, C.; Eck, T.F.; Ahmad, S.P.; Banerjee, B.P. Prairie grassland bidirectional reflectance measured by different instruments at the fife site. *J. Geophys. Res.: Atmos.* **1992**, *97*, 18887–18903.
34. Kimes, D.S. Dynamics of directional reflectance factor distributions for vegetation canopies. *Appl. Opt.* **1983**, *22*, 1364–1372.
35. Kimes, D.S.; Sellers, P.J. Inferring hemispherical reflectance of the earth's surface for global energy budgets from remotely sensed nadir or directional radiance values. *Remote Sens. Environ.* **1985**, *18*, 205–223.
36. Diner, D.J.; Beckert, J.C.; Reilly, T.H.; Bruegge, C.J.; Conel, J.E.; Kahn, R.A.; Martonchik, J.V.; Ackerman, T.P.; Davies, R.; Gerstl, S.A.W.; *et al.* Multi-angle imaging spectroradiometer (MISR) instrument description and experiment overview. *IEEE Trans. Geosci. Remote Sens.* **1998**, *36*, 1072–1087.
37. Jin, Y.; Schaaf, C.B.; Gao, F.; Li, X.; Strahler, A.H.; Lucht, W.; Liang, S. Consistency of MODIS surface bidirectional reflectance distribution function and albedo retrievals: 1. Algorithm performance. *J. Geophys. Res.: Atmos.* **2003**, *108*, 4158.
38. Bacour, C.; Breon, F.M. Variability of biome reflectance directional signatures as seen by polder. *Remote Sens. Environ.* **2005**, *98*, 80–95.
39. Jiao, Z.; Hill, M.J.; Schaaf, C.B.; Zhang, H.; Wang, Z.; Li, X. An anisotropic flat index (AFX) to derive BRDF archetypes from MODIS. *Remote Sens. Environ.* **2014**, *141*, 168–187.
40. Jiao, Z.; Zhang, H.; Dong, Y.; Schaaf, C.; Wang, Z.; Liu, Q.; Xiao, Q.; Li, X. An algorithm for retrieval of surface albedo from small view-angle airborne observations through the use of BRDF archetypes as prior knowledge. *IEEE J. Sel. Top. Appl. Earth Obs. Remote Sens.* **2015**, *2015*, doi:10.1109/JSTARS.2015.2414925.
41. Vermote, E.F.; El Saleous, N.Z.; Justice, C.O. Atmospheric correction of MODIS data in the visible to middle infrared: First results. *Remote Sens. Environ.* **2002**, *83*, 97–111.
42. Roujean, J.-L.; Leroy, M.; Deschamps, P.-Y. A bidirectional reflectance model of the earth's surface for the correction of remote sensing data. *J. Geophys. Res.* **1992**, *97*, 20455–20468.

43. Wanner, W.; Li, X.; Strahler, A.H. On the derivation of kernels for kernel-driven models of bidirectional reflectance. *J. Geophys. Res.* **1995**, *100*, 21077–21089.
44. Ross, J.K. *The Radiation Regime and Architecture of Plant Stands*; Kluwer Academic Publishers: Dordrecht, The Netherlands, 1981.
45. Li, X.; Strahler, A.H. Geometric-optical bidirectional reflectance modeling of the discrete crown vegetation canopy: Effect of crown shape and mutual shadowing. *IEEE Trans. Geosci. Remote Sens.* **1992**, *30*, 276–292.
46. Vermote, E.; Justice, C.O.; Breon, F.M. Towards a generalized approach for correction of the BRDF effect in MODIS directional reflectances. *IEEE Trans. Geosci. Remote Sens.* **2009**, *47*, 898–908.
47. Shuai, Y.; Masek, J.G.; Gao, F.; Schaaf, C.B. An algorithm for the retrieval of 30-m snow-free albedo from Landsat surface reflectance and MODIS BRDF. *Remote Sens. Environ.* **2011**, *115*, 2204–2216.

© 2015 by the authors; licensee MDPI, Basel, Switzerland. This article is an open access article distributed under the terms and conditions of the Creative Commons Attribution license (<http://creativecommons.org/licenses/by/4.0/>).